Series of Lanthanide-Alkali Metal-Organic Frameworks Exhibiting Luminescence and Permanent Microporosity

Brett D. Chandler, Joanne O. Yu, David T. Cramb,* and George K. H. Shimizu*

Department of Chemistry, University of Calgary, Calgary, Alberta, T2N 1N4, Canada

Received April 3, 2007. Revised Manuscript Received June 21, 2007

A series of permanently porous luminescent lanthanide frameworks of the general formula, $[Na_6(H_2O)_6][Ln(L)_4](H_2O)_nCl$, Ln = Sm (**1**), Eu (**2**), Gd (**3**), Tb (**4**), and Dy (**5**), have been prepared by the reaction of trivalent lanthanide salts with sodium-4,4′-disulfo-2,2′-bipyridine-*N*,*N*′-dioxide, L. The structures are formed via the one-pot self-assembly of the anionic cubic metalloligand, $[Ln(L)_4]^{5-}$, and subsequent cross-linking with sodium cations and chloride to afford a three-dimensional network with two-dimensional channels. The cross-linking units involve $[Na_4Cl]^{3+}$ clusters which resemble ideal faces of the halite structure. Both coordinated and uncoordinated water molecules, up to ∼80%, can be reversibly removed from **1**−**5** as identified using thermal gravimetric analysis/differential scanning calorimetry (TGA/DSC) leaving a rigid and porous framework with a Dubinin−Radushkevich (DR) surface area of 426 m^2/g determined using CO_2 adsorption. The permanent microporosity of the framework is also supported by the energy level splitting in the luminescence spectra which are maintained in both the hydrated and mostly dehydrated frameworks. Compounds **1**−**5** were each characterized by X-ray crystallography, TGA/DSC, water and CO_2 sorption analyses, and luminescence spectroscopy.

Introduction

Metal-organic frameworks (MOFs) continue to be an active area of research with an impetus on the coupling of desirable framework features with specific functional properties to create robust and/or dynamic materials.[1,2] With respect to sensor development, the coupling of a porous MOF with a luminescent phosphor is highly attractive as it provides a direct route to the development of robust and tunable sensing materials. Lanthanide-containing MOFs are highly attractive in this regard due their unique photophysical characteristics.[3,4] Until recently, only a handful of examples have been reported that combine porosity with the intrinsic luminescent properties of the lanthanide due to the difficulty in synthesizing such compounds.[5] While the higher coordination numbers of the lanthanide metals predispose them to the formation of high-dimensional frameworks, the flexible and irregular coordination geometries restrict the level of control in the preparation of the lanthanide complexes and often result in densely packed structures. Therefore, the development of rational synthetic routes for the construction of structurally well-defined solids is the most important factor for the creation of porous lanthanide-based MOFs.

One approach to circumvent the formation of nonporous lanthanide MOFs is to use a stepwise or *Aufbau* approach using metal-containing assemblies commonly referred to as metalloligands (Scheme 1). Altering the choice of ligand and stoichiometry used in the metalloligand formation dictates the resulting geometry and direction of polymer extension. Multidimensional frameworks can then be formed by subsequently cross-linking the metalloligands with secondary metal cations such as transition metals[6] or alkali/alkaline earth metals.[7] Judicious choice of ligand is required to ensure that

* Corresponding authors. E-mail: dcramb@ucalgary.ca (D.T.C.); gshimizu@ucalgary.ca (G.K.H.S.).

(1) (a) Kepert, C. J. *Chem. Commun.* **2006**, 695−700. (b) Ferey, G.; Mellot-Draznieks, C.; Serre, C.; Millange, F.; Dutour, J.; Surble, S.; Margiolaki, I. *Science* **2005**, *309*, 2040−2042. (c) Chae, H. K.; Siberio-Perez, D. Y.; Kim, J.; Go, Y.; Eddaoudi, M.; Matzger, A. J.; O'Keeffe, M.; Yaghi, O. M. *Nature* **2004**, *427*, 523−527. (d) Zhao, X. B.; Xiao, B.; Fletcher, A. J.; Thomas, K. M.; Bradshaw, D.; Rosseinsky, M. J. *Science* **2004**, *306*, 1012−1015. (e) Liu, Y.; Eubank, J. F.; Cairns, A. J.; Eckert, J.; Kravtsov, V. C.; Luebke, R.; Eddaoudi, M. *Angew. Chem. Int. Ed.* **2007**, *46*, 3278−3283.

(2) (a) Zhang, J. P.; Horike, S.; Kitagawa, S. *Angew. Chem., Int. Ed.* **2007**, *46*, 889−892. (b) Maji, T. K.; Matsuda, R.; Kitagawa, S. *Nat. Mater.* **2007**, *6*, 142−148. (c) Serre, C.; Mellot-Draznieks, C.; Surble, S.; Audebrand, N.; Filinchuk, Y.; Ferey, G. *Science* **2007**, *315*, 1828−1831. (d) Bradshaw, D.; Warren, J. E.; Rosseinsky, M. J. *Science* **2007**, *315*, 977−980. (e) Horike, S.; Matsuda, R.; Tanaka, D.; Matsubara, S.; Mizuno, M.; Endo, K.; Kitagawa, S. *Angew. Chem., Int. Ed.* **2006**, *45*, 7226−7230. (f) May, L. J.; Shimizu, G. K. H. *Z. Kristallogr.* **2005**, *220*, 364−372. (g) Kitagawa, S.; Uemura, K. *Chem. Soc. Rev.* **2005**, *34*, 109−119. (h) Shimizu, G. K. H. *J. Solid State Chem.* **2005**, *178*, 2519−2526.

(3) (a) Hill, R. J.; Long, D.-L.; Hubberstey, P.; Schroeder, M.; Champness, N. R. *J. Solid State Chem.* **2005**, *178*, 2414−2419. (b) Xia, J.; Zhao, B.; Wang, H.-S.; Shi, W.; Ma, Y.; Song, H.-B.; Cheng, P.; Liao, D.-Z.; Yan, S.-P. *Inorg. Chem.* **2007**, *46*, 1259−1267. (c) Mahata, P.; Natarajan, S. *Inorg. Chem.* **2007**, *46*, 1250−1258. (d) de Lill, D. T.; Cahill, C. L. *Chem. Commun.* **2006**, 4946−4948.

(4) Sabbatini, N.; Guardigli, M.; Lehn, J. M. *Coord. Chem. Rev.* **1993**, *123*, 201−28.

(5) (a) Zhu, W.-H.; Wang, Z.-M.; Gao, S. *Inorg. Chem.* **2007**, *46*, 1337−1342. (b) Zhang, L.-Z.; Gu, W.; Li, B.; Liu, X.; Liao, D.-Z. *Inorg. Chem.* **2007**, *46*, 622−624. (c) Zhu, W.-H.; Wang, Z.-M.; Gao, S. *Dalton Trans.* **2006**, 765−768. (d) Wong, K.-L.; Law, G.-L.; Yang, Y.-Y.; Wong, W.-T. *Adv. Mater.* **2006**, *18*, 1051−1054. (e) Pan, L.; Adams, K. M.; Hernandez, H. E.; Wang, X.; Zheng, C.; Hattori, Y.; Kaneko, K. *J. Am. Chem. Soc.* **2003**, *125*, 3062−3067. (f) Reineke, T. M.; Eddaoudi, M.; Fehr, M.; Kelley, D.; Yaghi, O. M. *J. Am. Chem. Soc.* **1999**, *121*, 1651−1657.

(6) (a) Liu, W.; Jiao, T.; Li, Y.; Liu, Q.; Tan, M.; Wang, H.; Wang, L. *J. Am. Chem. Soc.* **2004**, *126*, 2280−2281. (b) Ren, Y.-P.; Long, L.-S.; Mao, B.-W.; Yuan, Y.-Z.; Huang, R.-B.; Zheng, L.-S. *Angew. Chem., Int. Ed.* **2003**, *42*, 532−535. (c) He, Z.; He, C.; Gao, E.-Q.; Wang, Z.-M.; Yang, X.-F.; Liao, C.-S.; Yan, C.-H. *Inorg. Chem.* **2003**, *42*, 2206−2208. (d) Jian, L.; Shen, E.; Li, Y.; Xiao, D.; Wang, E.; Xu, L. *Cryst. Growth Des.* **2005**, *5*, 65−67.

10.1021/cm070930i CCC: $37.00
Published on Web 08/02/2007

Scheme 1. In-Situ Assembly Process of Lanthanide-Based Metalloligands

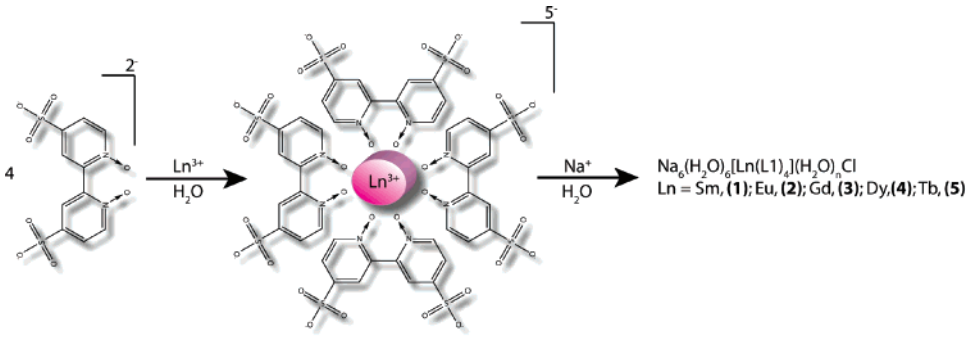

the chosen lanthanide metal is well-shielded from the surrounding environment to prevent quenching of the excited state and enhance its emission. Derivatives of 2,2′-bipyridine are known to be well-suited for the sensitization of europium and terbium cations allowing for the facile emission of visible light via *f*−*f* transitions.[8,9] Recently, we demonstrated that the formation of a nonsymmetrical, unsaturated metalloligand using three equivalents of 4,4′-disulfo-2,2′-bipyridine-*N*,*N*′-dioxide, L, followed by subsequent cross-linking using barium cations, can generate luminescent porous frameworks.[10] Recent MOF syntheses incorporating the cross-linking of saturated metalloligands containing transition metals have also been shown to be a viable synthetic route in the formation of porous frameworks.[11] Herein, we present the construction of a new series of robust and permanently porous frameworks using four equivalents of L to form anionic cubic metalloligands, $[Ln(L)_4]^{5-}$, (where Ln = Sm (**1**), Eu (**2**), Gd (**3**), Tb (**4**), and Dy (**5**)) that are subsequently cross-linked into three-dimensional luminescent architectures using sodium chloride clusters. The sodium-chloride clusters in this work resemble ideal faces of solid NaCl and impart great stability to the framework. While sulfonate complexes of divalent alkaline earth ions have demonstrated sorptive properties and ion exchange, no sulfonate salts of monocations have shown any porosity although some have shown reversible guest sorption properties.[12] Therefore, this work is the first example of a permanently porous sulfonate framework using metals that are monocationic. As well, it represents the first use of a lanthanide-based, cubic metalloligand to form a porous coordination framework.

Experimental Section

Synthesis and Characterization. $EuCl_3 \cdot 6H_2O$, $SmCl_3 \cdot 6H_2O$, $DyCl_3 \cdot 6H_2O$, $TbCl_3 \cdot 6H_2O$, and $GdCl_3 \cdot 6H_2O$ (99%) were obtained from Aldrich Chemical Co. and used as received. Sodium-4,4′-disulfo-2,2′-bipyridine-*N*,*N*′-dioxide was synthesized and purified based on a previously reported procedure.[13] Compounds **1**−**5** were prepared via vapor diffusion methods. In a typical synthesis, for compound **1**, sodium-4,4′-disulfo-2,2′-bipyridine-*N*,*N*′-dioxide (0.1 g, 0.233 mmol) was dissolved in water (5 mL). This ligand solution was then added to 6 N hydrochloric acid (100 μL) containing $SmCl_3 \cdot 6H_2O$ (21.3 mg, 0.058 mmol) dissolved in water (5 mL). The mixed ligand and metal solution was refluxed for 5 min and cooled to room temperature. Single crystals were grown by vapor diffusion of acetone into this solution. Between 1 and 3 weeks, crystals of **1**−**5** of sufficient size and quality were obtained for X-ray analysis.

Single-Crystal X-ray Diffraction. All single-crystal diffraction experiments were conducted at 173 K unless otherwise noted. Single crystals were collected using an Enraf-Nonius diffractometer with graphite monochromatic Mo Kα radiation (= 0.71069 Å) and equipped with a charge-coupled device (CCD) detector. The intensity data collection was performed in the $\omega\Phi$ scanning mode with the goniometer and detector angular settings optimized using the program COLLECT.[14] The crystal-to-detector distance was 30 mm for all data collections. The unit cell and the orientation matrix were refined using the entire data set of reflections. The diffraction spots were measured in full with a high accuracy, scaled with SCALEPACK,[14] corrected for Lorentz-polarization correction, and integrated using DENZO.[14] Structure solutions (SIR97)[15] and refinements (SHELXL-97)[16] were run in the space groups $P\bar{4}$ for all lanthanide-containing structures. The structure model (excluding hydrogen atoms) was readily obtained from successive difference Fourier maps. All aromatic hydrogen atoms were placed using AFIX 43. Hydrogen atoms were placed on well-defined water molecules from the difference map when the quality of data would permit, while hydrogen atoms were omitted from disordered water molecules entirely. In the final cycles of refinement, anisotropic displacement parameters and extinction coefficients were allowed to vary.

Thermal Gravimetric Analysis and Differential Scanning Calorimetry (TGA/DSC). Thermal gravimetric analyses (TGA) was carried out in a nitrogen atmosphere using a Netzsch STA449C

(7) (a) Deacon, G. B.; Gitlits, A.; Zelesny, G.; Stellfeldt, D.; Meyer, G. *Z. Anorg. Allg. Chem.* **1999**, *625*, 764−772. (b) Sun, H.-Y.; Huang, C.-H.; Jin, X.-L.; Xu, G.-X. *Polyhedron* **1995**, *14*, 1201−6.
(8) Wu, J.-Y.; Yeh, T.-T.; Wen, Y.-S.; Twu, J.; Lu, K.-L. *Cryst. Growth Des.* **2006**, *6*, 467−473.
(9) (a) Mukkala, V. M.; Kankare, J. J. *Helv. Chim. Acta* **1992**, *75*, 1578−1592. (b) Balzani, V.; Lehn, J. M.; Vandeloosdrecht, J.; Mecati, A.; Sabbatini, N.; Ziessel, R. *Angew. Chem., Int. Ed.* **1991**, *30*, 190−191.
(10) (a) Chandler, B. D.; Cramb, D. T.; Shimizu, G. K. H. *J. Am. Chem. Soc.* **2006**, *128*, 10403−10412. (b) Chandler, B. D.; Côté, A. P.; Cramb, D. T.; Hill, J. M.; Shimizu, G. K. H. *Chem. Commun.* **2002**, 1900−1901.
(11) (a) Cheng, A.-L.; Liu, N.; Zhang, J.-Y.; Gao, E.-Q. *Inorg. Chem.* **2007**, *46*, 1034−1035. (b) Zou, R.-Q.; Sakurai, H.; Xu, Q. *Angew. Chem., Int. Ed.* **2006**, *45*, 2542−2546. (c) Murphy, D. L.; Malachowski, M. R.; Campana, C. F.; Cohen, S. M. *Chem. Commun.* **2005**, 5506−5508. (d) Halper, S. R.; Do, L.; Stork, J. R.; Cohen, S. M. *J. Am. Chem. Soc.* **2006**, *128*, 15255−15268.
(12) (a) May, L. J.; Shimizu, G. K. H. *Chem. Mater.* **2005**, *17*, 217−220. (b) Makinen, S. K.; Melcer, N. J.; Parvez, M.; Shimizu, G. K. H. *Chem.*−*Eur. J.* **2001**, *7*, 5176−5182.
(13) Anderson, S.; Constable, E. C.; Seddon, K. R.; Turp, J. E.; Baggott, J. E.; Pilling, M. J. *J. Chem. Soc., Dalton Trans.* **1985**, 2247−61.
(14) *COLLECT*, *DENZO*, *SCALEPACK*, *SORTAV*, *Kappa CCD Program Package*; Delft, The Netherlands, 1998.
(15) Altomare, A.; Burla, M. C.; Camalli, M.; Cascarano, G. L.; Giacovazzo, C.; Guagliardi, A.; Moliterni, A. G. G.; Polidori, G.; Spagna, R. *J. Appl. Crystallogr.* **1999**, *32*, 115−119.
(16) Sheldrick, G. M. *SHELXL-97*, *Program for crystal structure refinement*; University of Gottingen: Germany, 1997.

Table 1. Crystallographic Data for Compounds 1−5

compound	1	2	3	4	5
formula sum	$C_{40}H_{24}SmC1N_8O_{46}Na_6S_8$	$C_{40}H_{24}EuClN_8O_{48}Na_6S_8$	$C_{40}H_{24}GdClN_8O_{48}Na_6S_8$	$C_{40}H_{24}TbClN_8O_{46}Na_6S_8$	$C_{40}H_{24}DyClN_8O_{47}Na_6S_8$
formula weight	1932.38	1966.59	1971.87	1941.55	1961.12
crystal system	tetragonal	tetragonal	tetragonal	tetragonal	tetragonal
space group	$P\bar{4}$ (no 81)	$P\bar{4}$ (no 81)	$P\bar{4}$ (no 81)	$P\bar{4}$ (no 81)	$P\bar{4}$ (no 81)
a (Å)	12.238(5)	12.265(5)	12.234(5)	12.245(5)	12.213(5)
b (Å)	12.238(5)	12.265(5)	12.234(5)	12.245(5)	12.213(5)
c (Å)	12.398(5)	12.412(5)	12.373(5)	12.407(5)	12.345(5)
α (deg)	90	90	90	90	90
β, (deg)	90	90	90	90	90
γ, (deg)	90	90	90	90	90
V, (Å^3)	1856.8(7)	1868.5(13)	1851.9(13)	1860.3(13)	1841.3(13)
Z	1	1	1	1	1
F_{000}	961	978	979	964	973
D_{calc} (g cm^{-3})	1.729	1.748	1.768	1.733	1.768
μ (mm^{-1})	1.193	1.243	1.303	1.352	1.422
λ (Å)	0.71069	0.71069	0.71069	0.71069	0.71069
GOF	1.028	1.055	1.061	1.194	1.053
Flack	0.5065	0.5007	0.0512	0.0219	−0.0068
σ Flack	0.0256	0.0156	0.0152	0.0123	0.0093
^aR %	7.64	5.54	6.48	5.28	4.05
^bR_w %	10.12	6.10	7.43	5.91	4.50

Jupiter analyzer with heating and cooling rates of 5 K/min. Vapor sorption experiments were performed on the TGA using the following procedure. Samples were heated for 3 h at 120 °C until desolvation was complete, and they were cooled to room temperature for 2 h. Water uptake experiments were performed by passing a stream of nitrogen over water at a flowrate of 50 mL/min for 1 h and 30 min at 24 °C and passing this "wet" gas into the sample chamber. Finally, the sample was purged with dry nitrogen for an additional 2 h to remove any surface-adsorbed water and reach full equilibration at 25 °C. This process was then repeated over multiple cycles to test the reproducibility of uptake.

Porosity Characterization. Surface area determination was performed via CO_2 sorption measurements using a Quantachrome Instruments Autosorb 1 surface area and pore size analyzer at 0 °C after outgassing at 120 °C for 12 h and using a cross-sectional area of 21 Å^2 for CO_2. Quantification of the surface area was performed using the Dubinin−Radushkevich (DR) equation.

Photophysical Characterization. Room-temperature phosphorescence measurements and lifetime determinations were carried out using a Varian Cary Eclipse fluorescence spectrophotometer with excitation and emission slit widths of 2.5 nm spectral resolution. Solid samples were suspended on a brass pin using Paratone oil as an adhesive. Lifetime data collection proceeded using a single flash with a delay of 100 μs, a gate time of 500 μs, and a decay of 5 ms unless otherwise noted. Lifetime data were fit using a first-order single exponential with a good quality of fit based on the reduced χ-square statistics.

Results and Discussion

Structure. Compounds **1**−**5** represent an isostructural series of three-dimensional porous frameworks and crystallize in the non-centrosymmetric tetragonal space group $P\bar{4}$ (Table 1). Compound **2**, the Eu analogue, will be used as a representative example for structural description. The three-dimensional structural motif of **2** arises from the initial formation of the anionic tetrakis-bipyridyl-*N*-oxide lanthanide metalloligands, $[Ln(L)_4]^{5-}$, which are subsequently cross-linked through the sulfonate groups by sodium ions and sodium chloride clusters. The eight coordinate lanthanide cations are chelated in a bidentate fashion by four L molecules resulting in a mildly distorted square antiprismatic geometry. The sulfonate groups are oriented on the periphery of the metalloligand in a distorted cubic geometry. The distortion arises from a single edge containing two corner vertices being lowered by 28.1(2)° relative to the rest of the cube (Figure 1a). The cubic metalloligands are cross-linked via sodium cations and NaCl clusters into elliptically shaped two-dimensional pores, 9.93 Å × 5.05 Å, running along the *a* and *b*-axes in the three-dimensional structure (Figure 1b).

Looking at the cross-linking more closely, the first sodium cation, Na1, is a minimally distorted octahedron. Two sulfonate oxygen atoms, O3, from two different ligands are situated trans to one another, Na1−O3 = 2.33(5) Å, while two additional sulfonate oxygen atoms from two separate ligands are cis with respect to each other, Na1−O6 = 2.48(6) Å. The remaining two sites on Na1 are occupied by two symmetry related water molecules, Na1−O1S = 2.37(7) Å, which bridge Na1 and Na2 metal centers. The second sodium cation, Na2, is involved in forming the NaCl cluster. Na2 is also seven-coordinated and ligated by three sulfonate groups, two unique water molecules and a chloride anion. One oxygen atom from each of the two sulfonate groups bind Na2, Na2−O5 = 2.41(5) Å, while the remaining sulfonate group employs two oxygen atoms, Na2−O6 = 2.55(6) Å and Na2−O8 = 2.41(5) Å, in a chelating mode. The coordination between the sodium cations, Na2, and chloride anions, Cl1, is of particular interest due to the aggregate that results and the effect such a motif has on the resultant framework. In the extended structure, each chloride anion sits in the center of a square plane formed by four Na2 atoms (Na2−Cl = 2.72(2) Å, Figure 2a). This motif, with respect to both symmetry and distances, is nearly identical to one face of the NaCl halite structure (Na−Cl = 2.81(4) Å).[17] Above and below this plane, coordinated and non-coordinated water molecules are present. Compound **1** differs slightly from **2**−**5** in that the chloride anion is disordered between two positions 0.68(0) Å directly above and below the square plane of sodium atoms. Thus, it is a slight

(17) Abrahams, S. C.; Bernstein, J. L. *Acta Cryst.* **1965**, *18*, 926−32.

deviation from the ideal halite motif observed in compounds **2**−**5**. The halite motif, Na_4Cl^{3+}, has, to date, only been observed in purely inorganic systems; therefore, this is the first observation of this structural motif in a metal-organic framework. The Na_4Cl^{3+} "halitelike" aggregates clearly represent a very stable building unit and are important not only in an electrostatic role but also as rigid spacers between the Ln metalloligands. Eight such units link to the sulfonate groups of a single metalloligand (Figure 2b) to enable the permanent porosity of the framework. This is fundamentally different from our previous work in which we reported the stepwise assembly of a different anionic metalloligand, $[Ln(L)_3(H_2O)_2]^{3-}$, to create a porous framework.[10] The 3:1 ligand to metal ratio was specifically chosen not to fill the coordination sphere as it was our notion that a 4-fold symmetric metalloligand would be predisposed to the formation of densely packed frameworks. However, spaced by the Na_4Cl^{3+} aggregates, the cubic metalloligands form not only an open structure but also a robust framework. Increasing the chloride concentration by the addition of 100 μL solution of 6 N hydrochloric acid favors the formation of the Na_4Cl^{3+} clusters due to the enhanced association of sodium and chloride ions in solution and subsequently produces larger crystals with an improvement in the overall yield. The 4:1 ligand:Ln ratio also efficiently shields the metals centers from closely diffusing water molecules resulting in an enhanced sensitization of the lanthanide due to a decrease in the vibronic quenching effects commonly observed with water.[18]

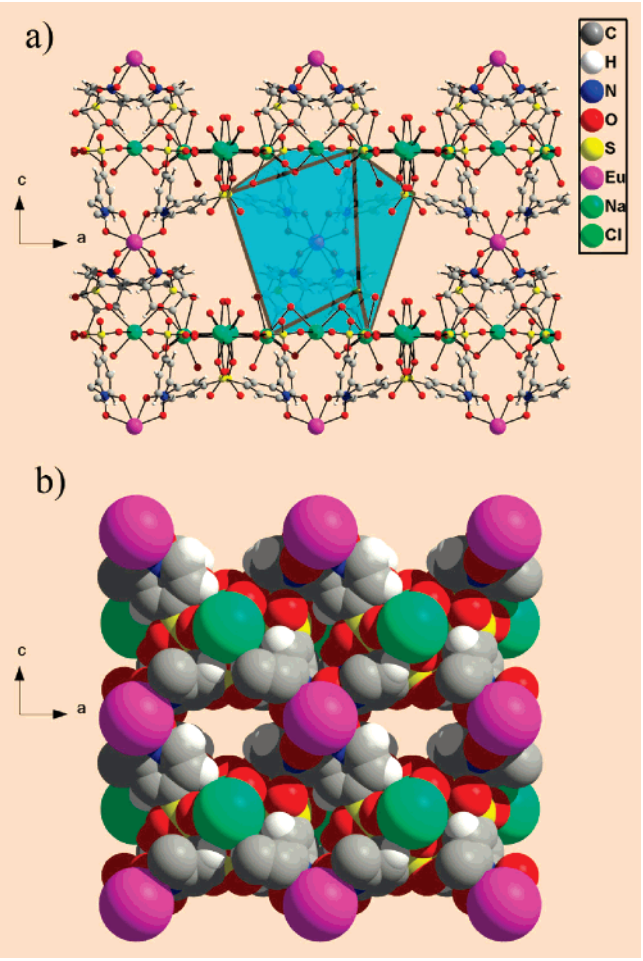

Figure 1. Extended framework view and structure components. All noncoordinating water molecules have been removed for clarity. (a) Ball and stick representation illustrating the distorted cubic building block, $[Ln(L)_4]^{5-}$, shown in blue with sulfonates comprising the vertices of the cube. (b) Space-filling diagram demonstrating the 9.9 Å × 5.0 Å hydrated channels.

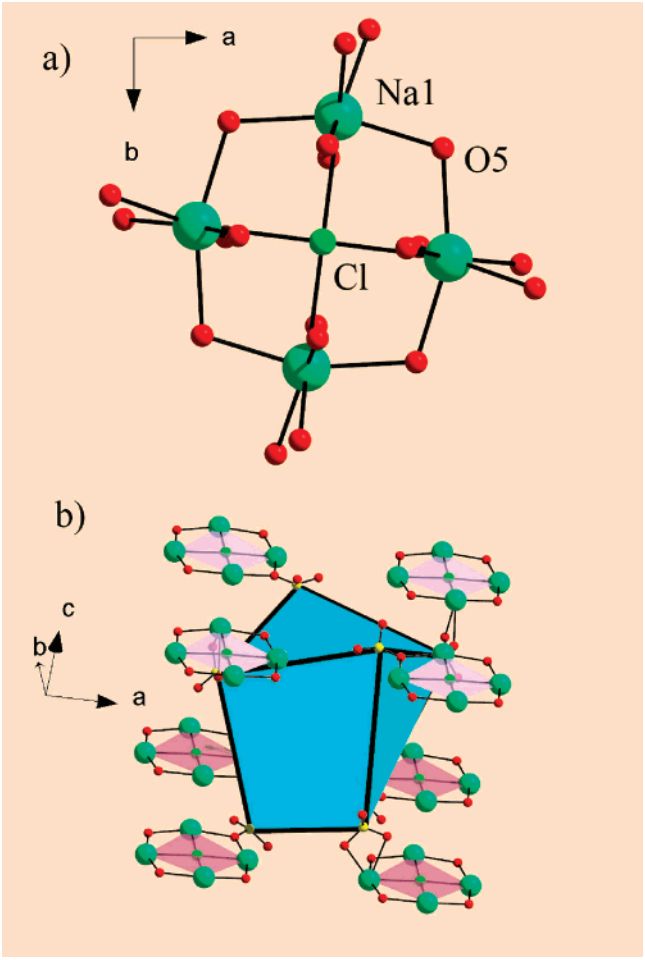

Figure 2. (a) Standard geometry of the Na_4Cl^{3+} sheets. The planar sheets are parallel to the *ab*-plane. (b) Illustration of the interaction between the cubic metalloligand (blue box) and the planar Na_4Cl^{3+} sheets. Each sulfonate coordinates to a single sheet giving a total of eight sheets per cube acting as rigid spacers between adjacent cubes.

Photophysical Characterization. A key advantage of the $[Ln(L)_4]^{5-}$ metalloligands is the incorporation of an intrinsic and efficient phosphor into the framework. The 2,2′-dipyridyl core of each ligand, L, has previously been established as a highly effective energy absorbing/transferring moiety and is therefore suitable for the sensitization of the lanthanides, particularly for Eu^{3+} and Tb^{3+} cations in compounds **2** and **4**, respectively.[4,9] Due to the sensitive nature of the electronic transitions of these metals, the emission spectra provide valuable information about the local environment of the metal. No detectible emission was observed for the Sm^{3+} or Dy^{3+} cations presumably due to the efficient deactivation pathway of the excited state through vibrational relaxation.[19] The europium emission spectrum obtained for compound **2** principally arises from transitions originating at the $^5D_0$ level. The strong emission is visibly detected at room temperature and ambient pressure (Figure 3). The emission spectrum

(18) Horrocks, W. D., Jr.; Sudnick, D. R. *J. Am. Chem. Soc.* **1979**, *101*, 334−40.
(19) Sastri, V. S.; Bunzli, J.-C.; Rao, V. R.; Rayudu, G. V. S.; Perumareddi, J. R. *Modern Aspects of Rare Earths and their Complexes*; Elsevier: New York, 2003.

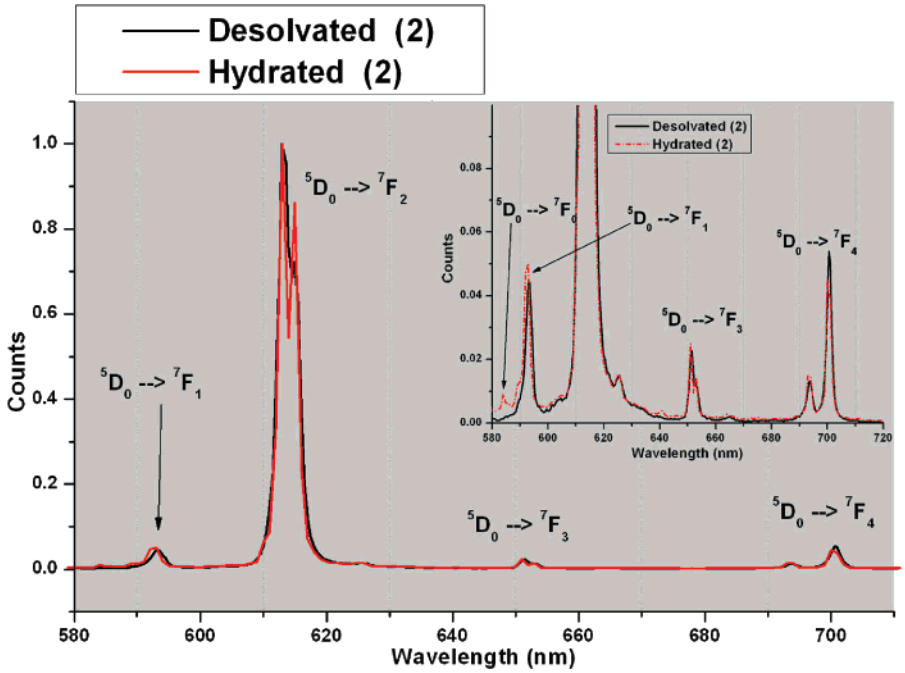

Figure 3. Stacked emission spectrum for the hydrated (red) and desolvated (black) phases for compound **2** excited at 330 nm. (inset) Magnified view of transitions demonstrating the nearly identical emission spectra.

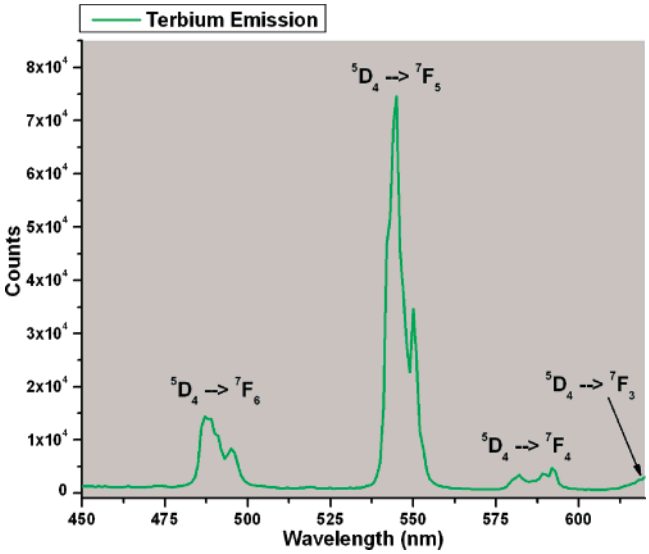

Figure 4. Terbium emission spectrum for compound **4**, excitation at 330 nm.

shows a weak band observed in the region of the $^5D_0 \rightarrow {}^7F_0$ transition. The $^5D_0 \rightarrow {}^7F_1$ is the second most intense transition; it consists of a single peak weakly split into two lines. The hypersensitive transition, $^5D_0 \rightarrow {}^7F_2$, consists of an intense band split into two sharp peaks. A less intense doublet of peaks is observed for the $^5D_0 \rightarrow {}^7F_3$ transition, while the $^5D_0 \rightarrow {}^7F_4$ transition is comprised of two well-defined peaks. The fluorescence spectrum collected for the terbium compound **4** is more complicated than that of **2** since an increased number of energy states are available due to the larger total angular momentum values in the ground-state manifold (Figure 4). The $^5D_4 \rightarrow {}^7F_6$ is the second largest peak observed and appears as a broad peak covering an 8 nm range. Closer inspection reveals a fine structure of four closely spaced peaks that decrease in intensity upon increasing frequency. Similar to the emission spectrum obtained for compound **2**, the dominant peak is the hypersensitive transition, $^5D_4 \rightarrow {}^7F_5$, which is made up of a single intense peak with a secondary shoulder at half the intensity. The $^5D_4 \rightarrow {}^7F_4$ transitions are made up of four weakly resolved peaks, and the $^5D_4 \rightarrow {}^7F_3$ transition appears as a single peak. The room-temperature phosphorescence lifetime of the europium and terbium complexes were determined to be 402 μs and 400 μs, respectively. The phosphorescent emission spectra for the samarium and dysprosium compounds yielded no discernible transitions; the emission intensities cannot be separated from the background. The lack of resolution and intensity from the emission spectra for compounds **1** and **5** is most likely due to the vibrational mixing of excited states.[19] These metals have a number of internal energy levels between the lowest emissive level, (Sm^{3+}: $^4G_{5/2}$, Dy^{3+}: $^4F_{9/2}$) and the ground state, (Sm^{3+}: $^6H_{5/2}$, Dy^{3+}: $^6H_{15/2}$) providing an efficient deactivation pathway of the excited state through vibrational relaxation.

The emission spectra obtained for compounds **2** and **4** consist predominantly of sharp well-defined transitions. As mentioned previously, the small splitting patterns that characterize each transition are useful for establishing the coordination number and the symmetry around the metal. Since the structural details are known for both compounds, the photophysical data complements the structural information and allows for a more complete understanding of the degree of ligand−lanthanide covalency. Europium spectra contain a greatly simplified fine structure compared to the other lanthanides making identification of the local site symmetry of the metal ion in the complex possible.[20] On the basis of the crystal data, the metal center exists in a mildly distorted square antiprismatic geometry resulting in a D_4 point symmetry based on the crystallographic data. When europium cations exist in a D_4 site symmetry, two compo-

(20) Forsberg, J. H. *Coord. Chem. Rev.* **1973**, *10*, 195−226.

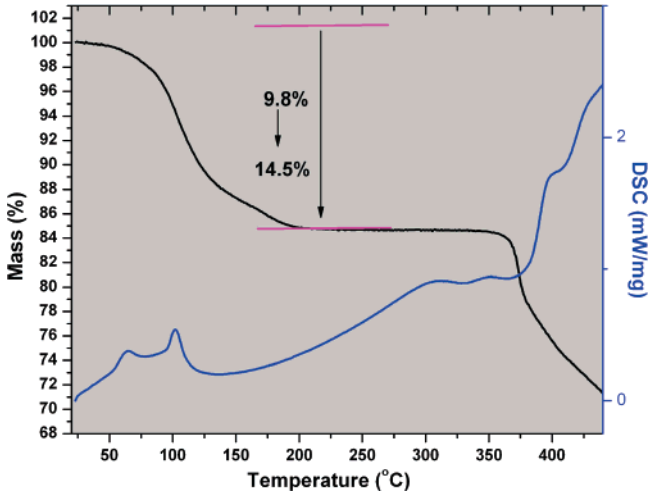

Figure 5. TGA loss of compound **2**. The red line is representative of the sample mass. The percentage values correlate to the range of mass losses observed for compounds **1**−**5**.

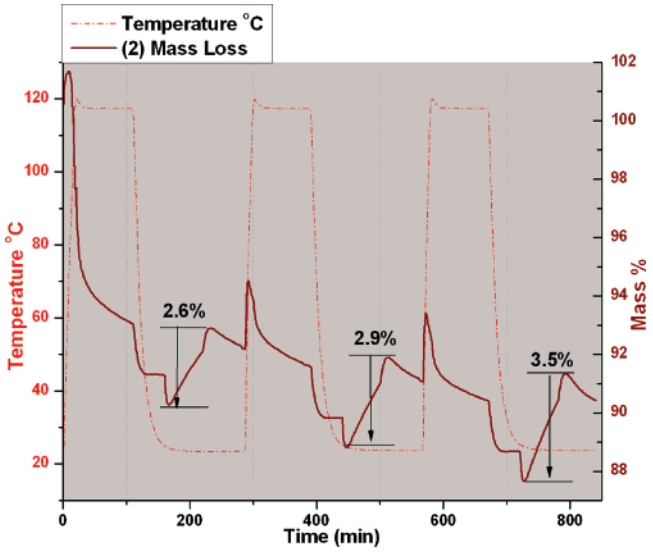

Figure 6. Reversible water vapor sorption for compound **2**. The dashed curve represents the heating cycle while the solid line indicates the concurrent mass loss. Percentage values indicate net uptake of water each cycle during the hydrating stage using a stream of "wet" N_2.

nents for the $^5D_0 \rightarrow {}^7F_1$ and one component of the $^5D_0 \rightarrow {}^7F_2$ are expected to be observed and the $^5D_0 \rightarrow {}^7F_0$ transitions remains strictly forbidden. While two peaks are observed for the $^5D_0 \rightarrow {}^7F_1$ transition, two well-resolved sharp peaks are seen on the hypersensitive transition indicating a small distortion from an ideal D_4 symmetry. The appearance of the $^5D_0 \rightarrow {}^7F_0$ transition is common when europium exists in a non-centrosymmetric ligand field allowing both electric-dipole and magnetic-dipole transitions to mix resulting in transitions to the "forbidden" state.[19] The $^5D_0 \rightarrow {}^7F_3$ and $^5D_0 \rightarrow {}^7F_4$ transitions are expected to consist of two peaks each of which is observed in the spectrum. On the basis of the experimental spectroscopic data collected, the emission spectra of compound **2** supports the crystallographic data explicitly and indicates that the metal is in an approximately D_4 point symmetry. Impressively, when the europium compound, **2**, is fully desolvated via thermal treatment, the emission spectrum remains nearly identical to the original. The stacked plot of the dehydrated and hydrated structures of **2** (inset of Figure 3) exhibits only small changes in the hypersensitive transition fine structure. Analysis of the weaker transitions in the spectra indicate that the forbidden $^5D_0 \rightarrow {}^7F_0$ transition is absent in the dehydrated structure, suggesting that water can perturb the ligand system to a minor extent inducing the non-centrosymmetric ligand field necessary for the forbidden transition to be observed. A lifetime of 399 μs was observed for the desolvated sample, indicating that the water in the channels does not directly affect the emission rate of the efficiently shielded europium cation. On the basis of these results, which indicate a minimal change in the ligand field of the lanthanide with dehydration, it is apparent that the overall topology of the network structure remains the same. This would require a permanently porous structure, and so, this was further examined through X-ray diffraction and gas sorption measurements.

Porosity. The thermal stability and robustness of compounds **1**−**5** was investigated using thermal gravimetric analysis (TGA, Figure 5). All the compounds exhibited very similar mass losses over the entire operating range. Initial loss of disordered water is observed up to 50 °C. At 50−120 °C, endothermic peaks (113.9 J/g) are observed in the DSC accompanying the loss of coordinated water molecules. At a heating rate of 5 °C/min, complete loss of solvent occurs between 120 and 200 °C with the total mass loss ranging from 9.8% to 14.5% which corresponds to 10.3−16.1 waters per unit cell for compounds **1**−**5**. Allowing for necessary differences in sampling and handling, this is in good agreement with the crystal data which suggests a value between 12 and 14 water molecules per unit cell. The samples reach a stable plateau from 200 °C until the decomposition of the frameworks at 360 °C with a concomitant exothermic peak in the DSC. Since compounds **1**−**5** contain two-dimensional channels, are thermally robust, and are permanently porous based on the lanthanide emission spectra, a water uptake study was performed using the TGA to demonstrate porosity via reversible uptake. A thermogram is shown in Figure 6 containing three dehydrating/rehydrating cycles for compound **2**. A 10% mass loss is observed during the first drying step which can be completed by heating at 120 °C over a period of 2 h. Upon cooling, a stream of nitrogen passed over 10 mL of water was introduced into the sample chamber. As evidenced from the change in mass, the sample does resorb water, although only approximately one-third of the initial amount lost. This process is repeatable multiple times with the net uptake increasing a small amount during each cycle. Thus, while the sample is able to resorb water, the kinetics of this process are slow at room temperature requiring longer loading times. To verify this, single crystals were fully dehydrated at 120 °C for 10 h followed by exposure to water vapor at room temperature for 24 h. Subsequent single-crystal X-ray diffraction analysis and structure determination revealed that the crystals had hydrated to their nascent form. The reversibility of this process demonstrates the robustness of the sample to the removal and introduction of water molecules into the framework. In order to analyze the dehydrated phase by crystallography, a single crystal of **2** was heated on the diffractometer and unit cells collected after heating at 50,

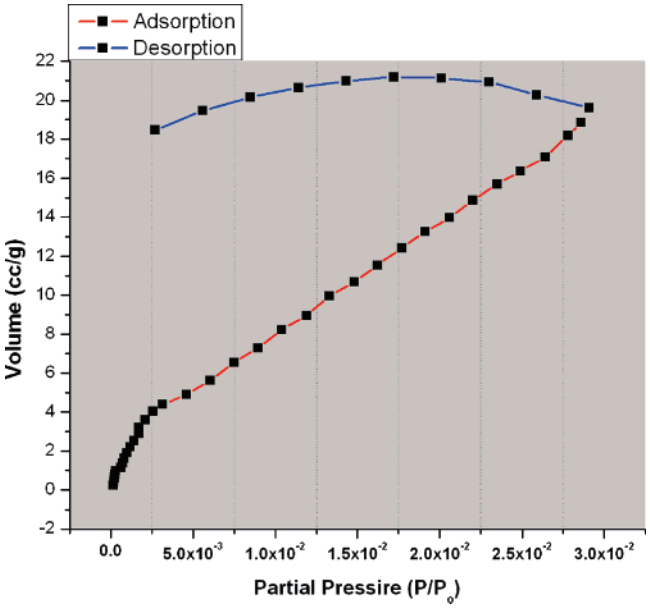

Figure 7. Carbon dioxide sorption isotherm for compound **2**. Adsorption is shown in red, while desorption is shown in blue.

100, 125 °C, and after holding at 125 °C for 8 h. Crystallinity is observed to 125 °C, but a gradual loss of order is observed over the 8 h heating period. This is consistent with the network structure being intact to ~80% of water removal. As mentioned above, at this stage and above, rehydration generates the unit cell of the nascent crystal. For the luminescence experiments, given the hygroscopic nature of the dried material, the samples would likely have partially rehydrated during the time frame of the experiment.

The porosity of compound **2** was further characterized by adsorption studies with CO_2 at 0 °C. The sample was degassed for 5 h at 120 °C under high vacuum. The adsorption (red) and desorption (blue) cycles are shown in Figure 7. As the crystal structure was known to be microporous in nature, the Dubinin−Radushkevich (DR) equation was used for data analysis of the experimental isotherm and gives a linear fit of the data throughout the entire adsorption range.[21] From the DR analysis, the surface area was determined to be 426 m^2/g, the micropore volume, 0.09 mL/g, and the average pore width, 1.20 nm, which is in good agreement with the crystal data.[22] Further validation of the DR model stems from the 21.5 kJ/mol adsorption energy which is typical for CO_2 physisorption. The observed rapid onset of CO_2 sorption at very low pressures is characteristic of the presence of micropores undergoing a volume-filling process. Therefore, the dry phase of **2** possesses a high degree of porosity. The desorption isotherm also shows a marked hysteresis which has been suggested to indicate dynamic flexibility with respect to metal organic frameworks.[23] On the basis of the high-temperature X-ray diffraction experiment, some structure shifting does take place at the ultimate stages of dehydration to yield a highly hygroscopic solid. On the basis of this data alone, it is difficult to assign the observed hysteresis to this shift or to nonequilibrated diffusion phenomena caused by adsorbate−adsorbate interactions between CO_2 molecules and pore-blocking effects of the connected pore topologies.[24]

Conclusions

In summary, we have demonstrated that a series of permanently porous luminescent frameworks can be formed through the formation of a rigid lanthanide metalloligand, $[Ln(L)_4]^{5-}$, in combination with halitelike Na_4Cl^{3+} aggregates generated in-situ. These halite units impart significant stability to the structure and, coupled with the metalloligand approach, enable the observation of permanent microporosity as confirmed by reversible hydration and a DR surface area of 426 m^2/g from CO_2 sorption experiments. Beyond the structural role that the metalloligand plays, the europium and terbium compounds, **2** and **4**, serve as useful and predictable phosphors. The emission spectra can be used in a diagnostic role to gain insight into the framework structure and properties as water is removed. These results further illustrate the utility of a stepwise assembly approach to the generation of functional MOFs both with regard to sustaining porous structures and for purposes of incorporating predictable physical properties. Future work will include an investigation of the selectivity of the frameworks to additional guests and the photophysical properties that result.

Acknowledgment. We acknowledge support from the Natural Sciences and Engineering Research Council (NSERC) of Canada for Discovery Grants to D.T.C. and G.K.H.S. and the Canadian Institute for Photonics Innovation (CIPI) for a grant to D.T.C.

Supporting Information Available: CIF files for **1**−**5** and details of complete characterization of **1**−**5**. This material is available free of charge via the Internet at http://pubs.acs.org.

CM070930I

(21) Rouquerol, F.; Rouquerol, J.; Sing, K. *Adsorption by Powders and Porous solids*; Academic Press: New York, 1999. (b) Dubinin, M. M. *Chem. Rev.* **1960**, *60*, 235−41.

(22) For other microporous Ln MOFs, see: (a) Evans, O. R.; Ngo, H. L.; Lin, W. *J. Am. Chem. Soc.* **2001**, *123*, 10395−10396. (b) Cui, Y.; Ngo, H. L.; Lin, W. *Inorg. Chem.* **2002**, *41*, 5940−5942.

(23) Kitagawa, S.; Kitaura, R.; Noro, S.-i. *Angew. Chem., Int. Ed.* **2004**, *43*, 2334−2375.

(24) (a) Fomkin, A. A. *Adsorption* **2005**, *11*, 425−436. (b) Thommes, M.; Smarsly, B.; Groenewolt, M.; Ravikovitch, P. I.; Neimark, A. V. *Langmuir* **2006**, *22*, 756−764.